Synthesis and Characterization of Biocompatible and Size-Tunable Multifunctional Porous Silica Nanoparticles

Synthesis and Characterization of Biocompatible and Size-Tunable Multifunctional Porous Silica Nanoparticles

Yu-Shen Lin and Christy L. Haynes*

Department of Chemistry, University of Minnesota, 207 Pleasant Street SE, Minneapolis, Minnesota 55455

Received May 6, 2009

In this work, size-controlled multifunctional mesoporous silica nanoparticles having large surface areas, embedded luminescence, high magnetization, and excellent aqueous dispersity have been successfully prepared by using a simple one-pot synthesis. The size and pore ordering of these particles can be easily controlled based on the number density of Fe_3O_4 nanoparticle nucleation sites introduced during the silica condensation reaction. Dissolution of the embedded Fe_3O_4 nanoparticles yields hollow mesoporous silica nanoparticles as well. These multifunctional porous nanoparticles were characterized by transmission electron microscopy, X-ray diffraction, nitrogen adsorption−desorption behavior, dynamic light scattering, zeta potential, magnetic susceptibility, and photoluminescence. Furthermore, in vitro 3-(4,5-dimethylthiazol-2-yl)-2,5-diphenyl-tetrazolium bromide (MTT) and hemolysis assays were performed to evaluate any unintended cytotoxicity. The biocompatibility of the multifunctional nanoparticles, even at very high doses, ensures their potential in biomedical applications.

Introduction

Since the first report of ordered mesoporous silica in 1992,[1] extensive work has been done exploring the syntheses, characterization, and application of these materials. Biomedical applications such as delivery of anticancer drugs,[2] enzymes,[3] and DNA[4] are among the most promising, exploiting the nanoparticles' ordered pore structure, large surface area, and considerable pore volume. The ideal biomedical nanoparticles (NPs) could be used simultaneously in diagnosis, imaging, and therapy. Toward this goal, several types of multifunctional nanomaterials have recently been reported in the literature, including plasmonic magnetic nanocrystals,[5−7] core−satellite nanocomposites,[8] and polymeric nanohybrids.[9,10] Mesoporous silica nanoparticles (MSNs) can also be used as a multifunctional platform, as has been demonstrated in several recent papers focusing on the synthesis of porous silica particles having fluorescent,

magnetic, cellular labeling, and/or therapeutic functions.[11−14] However, to date, the biomedical use of the MSN materials reported is hindered by either their tendency to aggregate upon exposure to physiological conditions[11,12] and/or overall large nanoparticle size, with particle diameters exceeding 150 nm.[13,14] Synthesized MSN size is critical because studies have shown that silica particles with diameters greater than 100 nm are rapidly taken up by the reticuloendothelial system (RES), accumulating in the liver and spleen before a loaded drug can be delivered to the target cells/tissue,[15,16] but that smaller silica NPs (< 50 nm diameter) with poly(ethylene glycol) (PEG) modification have significantly decreased uptake by RES organs and exhibit a longer blood circulation time.[17] Although well-ordered MSNs with diameters as low as 20 nm have been synthesized using a double surfactant system,[18] the resulting nanoparticles aggregate easily and, thus, discourage effort to incorporate other functionality such as magnetic contrast, because the base nanoparticle is not appropriate for biomedical use. In cases where attempts have been made to embed magnetic centers into MSNs, the synthesized materials suffer from

*To whom correspondence should be addressed. E-mail: chaynes@umn.edu.
(1) Kresge, C. T.; Leonowicz, M. E.; Roth, W. J.; Vartuli, J. C.; Beck, J. S. *Nature* **1992,** *359,* 710.
(2) Lu, J.; Liong, M.; Zink, J. I.; Tamanoi, F. *Small* **2007,** *8,* 1341.
(3) Slowing, I. I.; Trewyn, B. G.; Lin, V. S.-Y. *J. Am. Chem. Soc.* **2007,** *129,* 8845.
(4) Torney, F.; Trewyn, B. G.; Lin, V. S.-Y.; Wang, K. *Nat. Nanotechnol.* **2007,** *2,* 295.
(5) Lim, Y. T.; Cho, M. Y.; Kim, J. K.; Hwangbo, S.; Chung, B. H. *ChemBioChem* **2007,** *8,* 2204.
(6) Wang, L.; Bai, J.; Li, Y.; Huang, Y. *Angew. Chem., Int. Ed.* **2008,** *47,* 2439.
(7) Lim, J.; Eggeman, A.; Lanni, F.; Tilton, R. D.; Majetich, S. A. *Adv. Mater.* **2008,** *20,* 1721.
(8) Lee, J.-H.; Jun, Y.-W.; Yeon, S.-I.; Shin, J.-S.; Cheon, J. *Angew. Chem., Int. Ed.* **2006,** *45,* 8160.
(9) Yang, J.; Lee, C.-H.; Ko, H.-J.; Suh, J.-S.; Yoon, H.-G.; Lee, K.; Huh, Y.-M.; Haam, S. *Angew. Chem., Int. Ed.* **2007,** *46,* 8836.
(10) Kim, J.; Lee, J. E.; Lee, S. H.; Yu, J. H.; Lee, J. H.; Park, T. G.; Hayeon, T. *Adv. Mater.* **2008,** *20,* 478.

(11) Zhao, W.; Gu, J.; Zhang, L.; Chen, H.; Shi, J. *J. Am. Chem. Soc.* **2005,** *127,* 8916.
(12) Kim, J.; Lee, J. E.; Lee, J.; Yu, J. H.; An, B. C.; Kim, K.; Hwang, Y.; Shin, C. H.; Park, J. G.; Kim, J.; Hyeon, T. *J. Am. Chem. Soc.* **2006,** *128,* 688.
(13) Giri, S.; Trewyn, B. G.; Stellmaker, M. P.; Lin, V. S.-Y. *Angew. Chem., Int. Ed.* **2005,** *44,* 5038.
(14) Lin, Y.-S.; Wu, S.-H.; Hung, Y.; Chou, Y.-H.; Chang, C.; Lin, M.-L.; Tsai, C.-P.; Mou, C.-Y. *Chem. Mater.* **2006,** *18,* 5170.
(15) Wu, S.-H; Lin, Y.-S.; Hung, Y.; Chou, Y.-H.; Hsu, Y.-H.; Chang, C.; Mou, C.-Y. *ChemBioChem* **2008,** *9,* 53.
(16) Taylor, K. M. L.; Kim, J. S.; Rieter, W. J.; An, H.; Lin, W.; Lin, W. *J. Am. Chem. Soc.* **2008,** *130,* 2154.
(17) He, X.; Nie, H.; Wang, K.; Tan, W.; Wu, X.; Zhang, P. *Anal. Chem.* **2008,** *80,* 9597.
(18) Suzuki, K.; Ikari, K.; Imai, H. *J. Am. Chem. Soc.* **2004,** *126,* 462.

insufficient magnetic contrast achieved due to the low mass percentage ($< 1\%$) of incorporated magnetic nanoparticles or destruction of the well-ordered, high surface area character of the silica structure. The resulting low magnetic response is due to the thick mesoporous silica shell[12] or the large size of the mesoporous silica NP[14] and suggests that a large dose (e.g. 175 mg or 500 mg NPs/kg) would have to be injected to perform in vivo magnetic resonance imaging (MRI).[15,19] To date, these shortcomings largely limit the practical use for in vivo biomedical applications; to realize the full potential of multifunctional MSNs, a synthesis must be designed that produces small, easily dispersed, and well-ordered silica particles with higher mass percentage of incorporated magnetic centers. The great potential of these materials has generated significant efforts to achieve these goals by multiple research groups.[19,20] Recent efforts to achieve this goal include the work of Zhao and co-workers who reported a novel synthesis of a high-magnetization $Fe_3O_4@SiO_2$ particle with an ordered porous structure;[20] however, the relatively large size (> 500 nm diameter) limits its use for intravenous (iv) injected biological applications. Also, Hyeon and co-workers reported a novel synthesis of uniform multifunctional NPs with small size (~ 45 nm diameter) and high aqueous stability.[19] Unfortunately, these nanoparticles still have low magnetic response and disordered mesostructure, limiting their use for bioimaging, efficient drug loading, or bioseparations. Up to now, none of the reported materials possess the optimal characteristics: (1) small size (< 50 nm); (2) excellent aqueous dispersity; (3) ordered porous structure with high surface are (> 600 m^2/g); and (4) high magnetic response (> 10 emu/g) to facilitate drug delivery, bioseparation, and bioimaging applications. The most obvious solution to achieve the optimal characteristics is to reduce the overall silica NP size while maintaining the mesoporous structure.

In addition to design of ideal nanomaterials for nanotherapeutics, the unintentional toxicity of these NPs should be monitored as part of the design process. The 3-(4,5-dimethylthiazol-2-yl)-2,5-diphenyl-tetrazolium bromide (MTT) assay is widely used to study the cytotoxicity of various nanomaterials, and while it permits an NP to NP comparison, it gives insight only into changes in cell mitochondrial function. While there are four major routes of NP entry into the human body (inhalation, ingestion, transdermal penetration, and injection), biomedical NPs are most likely to be delivered via injection, and thus, blood compatibility is critical. Initial blood compatibility screens should monitor NP hemolytic activity, the ability of the NPs to lyse red blood cells, leading to anemia as well as more serious blood conditions. However, very few reports implement a hemolytic assay to study the cytotoxicity of various NPs.[21-23] In one very recent example, Slowing and co-workers examined the hemolytic activity of pristine MSNs in rat red blood cells and demonstrated promising results,[24] but these measurements should be pursued in clinically relevant human blood with the most promising multifunctional nanoparticles.

In this paper, we use ammonium hydroxide as a basic catalyst and one-pot synthesis conditions to produce size-tunable, sub-100-nm diameter, well-ordered multifunctional mesoporous silica NPs with sufficient magnetic loading and visible to near-infrared fluorescence that are stable and well-dispersed in aqueous solutions (designated as $Fe_3O_4@$Dye-MSNs@PEG, Dye = FITC, RITC, and DyLight 800). Furthermore, MTT and hemolysis assays are employed to assess the biocompatibility of the smallest synthesized $Fe_3O_4@$Dye-MSNs@PEG.

Experimental Section

Materials. All chemicals were used without further purification. *n*-Cetyltrimethylammonium bromide (CTAB, 99%), fluorescein isothiocyanate isomer I (FITC, 90%), rhodamine B isothiocyanate mixture of isomers (RITC), tetraethyl orthosilicate (TEOS, 98%), dimethyl sulfoxide (DMSO, 99.9%), and polyvinyl pyrrolidone (PVP, average MW 10 000 g/mol) were obtained from Sigma Aldrich. 3-Aminopropyl-trimethoxysilane (APTMS, 97%) was obtained from Fluka. [Hydroxy(polyethyleneoxy)propyl] triethoxysilane, (PEG-Silane, MW 575−750 g/mol, 50% in ethanol) was purchased from Gelest. 3-(4,5-Dimethylthiazol-2-yl)-2,5-diphenyl-tetrazolium bromide (MTT) was obtained from Invitrogen. Ammonium nitrate (99.9%), ammonium hydroxide (NH_4-OH, 28−30 wt % as NH_3), chloroform (99.8%), hydrochloric acid (HCl, 36.5−38%), and iron(III) chloride hexahydrate ($FeCl_3 \cdot 6H_2O$, $> 99\%$) were purchased from Mallinckrodt. DyLight 800 NHS ester (98−100%), iron(II) chloride tetrahydrate ($FeCl_2 \cdot 4H_2O$ 99−102%), and oleic acid were obtained from Fisher Scientific. Absolute anhydrous and 95% ethanol was purchased from Pharmco-Aaper. Ultrapure water was generated using a Millipore Milli-Q system with a Milli-pak filter of 0.22 μm pore size and used for all the preparation of aqueous solutions.

Preparation of Hydrophobic Magnetite (Fe_3O_4) NPs. The hydrophobic magnetite NPs were synthesized based on a slight modification of a published one-pot chemical coprecipitation method.[25] First, the deionized water was purged with nitrogen gas for 10 min. Then, 4.80 g of $FeCl_3 \cdot 6H_2O$, 2.00 g $FeCl_2 \cdot 4H_2O$, and 0.85 mL oleic acid were added to 30 mL of deionized water under nitrogen atmosphere with vigorous stirring. The mixture solution was heated to 90 °C. Then, 20 mL of ammonium hydroxide (14 wt %) was added rapidly to the solution, and it immediately turned black. The reaction was kept at 90 °C for 2.5 h and then allowed to cool to room temperature. The black precipitate was collected by centrifugation at 10 016*g* for 10 min and resuspended in chloroform with a end concentration of 54.5 mg oleic acid-capped Fe_3O_4/mL.

(19) Kim, J.; Kim, H. S.; Lee, N.; Kim, T.; Kim, H.; Yu, T.; Song, I. C.; Moon, W. K.; Hyeon, T. *Angew. Chem., Int. Ed.* **2008**, *47*, 8438.
(20) Deng, Y.; Qi, D.; Deng, C.; Zhang, X.; Zhao, D. *J. Am. Chem. Soc.* **2008**, *130*, 28.
(21) Jovanovic, A. V.; Flint, J. A.; Varshney, M.; Morey, T. E.; Dennis, D. M.; Duran, R. S. *Biomacromolecules* **2006**, *7*, 945.

(22) Koziara, J. M.; Oh, J. J.; Akers, W. S.; Ferraris, S. P.; Mumper, R. J. *Pharm. Res.* **2005**, *22*, 1821.
(23) Dorovolskaia, M. A.; Clogston, J. D.; Neun, B. W.; Hall, J. B.; McNeil, S. E. *Nano Lett.* **2008**, *8*, 2180.
(24) Slowing, I. I.; Wu, C.-W.; Vivero-Escoto, J. L.; Lin, V. S.-Y. *Small* **2009**, *5*, 57.
(25) Molday, R. S. Magnetic iron-dextran microspheres. U.S. Patent 4,452,773, **1984**.

Synthesis of PEG-Modified Fluorescent Mesoporous Silica NPs with Incorporated Fe₃O₄ NPs (Fe₃O₄@Dye-MSNs@PEG) and PEG-Modified Fluorescent Hollow Mesoporous Silica NPs (H-Dye-MSN): Dye = FITC, RITC, and DyLight 800. The preconjugated N-1-(3-trimethoxy-silylpropyl)-N-fluoresceyl thiourea (FITC-APTMS) was prepared by combining 5 μL of APTMS and 2 mL of 0.023 M FITC ethanolic solution under continuous stirring and dark conditions.[26] The RITC-APTMS was prepared in the same manner. In a typical synthetic procedure for 33-nm-diameter Fe₃O₄@FITC-MSNs@PEG, 1.2 mL of oleic acid-capped Fe₃O₄ nanoparticle solution was added to 5 mL of 0.16 M aqueous CTAB containing 0.2 g PVP10. The resulting solution was ultrasonicated at 42 kHz for 1 h to evaporate the chloroform, resulting in a transparent black solution. This solution was added to a 150 mL of 0.255 M ammonium hydroxide solution and heated to 50 °C. Then, 450 μL of FITC-APTMS and 3.0 mL of 0.88 M dilute ethanolic TEOS were added sequentially to the reaction solution under continuously stirring (600 rpm). After 30 min, 600 μL of PEG-silane was added, and the solution was allowed to stir for another 30 min. The solution was then aged at 50 °C for 24 h. The as-synthesized Fe₃O₄@FITC-MSNs@PEG solution was centrifuged at 53 300g for 30 min and, then, washed and redispersed in 50 mL of ethanol. To avoid the Fe₃O₄ dissolution that occurs under acidic conditions, the surfactants were removed using a fast and efficient ion exchange method where the as-synthesized Fe₃O₄@FITC-MSNs@PEG was transferred to 50 mL of ethanol containing 0.3 g of NH₄NO₃ and kept at 60 °C for 1 h.[27] The extraction step was repeated twice to completely remove the surfactants. To generate PEG-coated hollow fluorescent mesoporous silica NPs (H-FITC-MSNs@PEG), the Fe₃O₄ NPs and CTAB surfactants were removed using acidic ethanol (pH < 1.0) under reflux for 6 h. After the extraction, these NPs were washed three times with ethanol and redispersed/stored in 20 mL of ethanol. The Fe₃O₄@RITC-MSNs@PEG was obtained by substituting RITC-APTMS for FITC-APTMS in the previously mentioned reaction. For Fe₃O₄@DyLight800-MSNs@PEG, the Fe₃O₄@MSNs@PEG was prepared without the addition of dye. Then, the Fe₃O₄@MSNs@PEG was modified with APTMS at 60 °C for 6 h. The Fe₃O₄@DyLight800-MSNs@PEG was synthesized by adding 100 μL of 10 mg/mL N-hydroxysuccinimide (NHS)-ester-activated DyLight800 (dissolved in DMF) to an amine-functionalized Fe₃O₄@MSNs@PEG colloidal solution. The reaction was carried out in a Dulbecco's phosphate-buffered saline (DPBS, Gibco) at room temperature for 1 h. Once the coupling was complete, all purification and surfactant extraction followed the procedure described above. The solid products for XRD and BET characterizations were obtained by centrifugation followed by drying at 60 °C for 24 h.

Synthesis of Stöber SiO₂ NPs, PEG-Modified Stöber SiO₂ NPs (SiO₂@PEG), and Fe₃O₄@SiO₂. The detailed synthesis of these nonporous silica NPs is described in the Supporting Information. Herein, the PEG-modified Stöber SiO₂ NPs are referred to as SiO₂@PEG-12 and SiO₂@PEG-24 where the number indicates the PEG coating reaction time allowed in hours.

Cell Culture and MTT Viability Assay. The PC-12 pheochromocytoma cells (American type Culture Collection, ATCC, CRL-1721) were cultured at 37 °C under 5% CO₂ in RPMI-1640 media (Lonza) containing 10% horse serum (Invitrogen), 5%

fetal bovine serum (FBS, Sigma), and 1% penicillin/streptomycin (Gibco). The HeLa and HCT-116 cells (a generous gift from Professor Duncan Clarke, University of Minnesota) were cultured at 37 °C under 5% CO₂ in DMEM media (HyClone) supplemented with 10% FBS and 1% penicillin/streptomycin. All three cancer cell lines were used to screen cytotoxicity of 33 nm Fe₃O₄@FITC-MSN@PEG. Typically, 1×10^5 of cells per well were plated in 24-well plates for the MTT viability assay. After 24 h for cell attachment, the cells were incubated with varied concentrations of 33 nm diameter Fe₃O₄@FITC-MSNs@PEG NPs in media for 12 h. Then, the NP-treated cells were washed three times with 500 μL of PBS and allowed to incubate with MTT media (0.5 mg/mL) for 2 h at 37 °C. The formazan dye crystals generated by live cells were dissolved in DMSO, and the absorbance values at 570 nm were determined by using a microplate reader with absorbance at 655 nm as a reference. The cell viability was calculated by comparing the absorbance of a nanoparticle treated well to that of the control well.

Hemolysis Assay. Human blood was obtained from Memorial Blood Centers (St. Paul, MN). The whole blood was diluted to 1/10 of its original volume using calcium and magnesium-free DPBS solution. Red blood cells (RBCs) were isolated by centrifugation at 10 016g for 10 min, washed, and resuspended five times with PBS solution. Then 0.2 mL of diluted RBCs suspension was added to 0.8 mL of nanoparticle solution at different concentration and mixed by vortexing. Incubation of deionized water and DPBS with RBCs were used as positive control and negative control, respectively. All the samples were kept in static conditions at room temperature for 3 h. Finally, the mixtures were centrifuged at 10 016g for 3 min. The absorbance values of supernatants at 570 nm were determined by using a microplate reader with absorbance at 655 nm as a reference. The hemolysis percentage of RBCs was calculated based on the formula shown below.

Hemolysis percentage = ((sample absorbance − negative control absorbance)/(positive control absorbance − negative control absorbance)) × 100.

Characterization. Transmission electron microscopy (TEM) images were taken on a JEOL JEM-1210 microscope (operating at 120 kV). Samples were prepared on a Formvar-coated copper grid by evaporating one drop of diluted ethanolic suspension of the NPs. Image analysis was performed using SigmaScan Pro 5.0. Powder X-ray diffraction (XRD) was performed on a Bruker-AXS D-5005 (Siemens) X-ray diffractometer using filtered Cu Kα radiation (λ = 0.154 nm) at 45 kV and 20 mA. Data were collected by step scan with a step size of 0.018° and a step time of 1.0 s. Surface area, N₂ adsorption−desorption isotherms, and pore-size distributions were obtained using of an Autosorb-1 analyzer (Quantachrom Instruments) at 77 K. Prior to measurements, samples were degassed at 120 °C for 12 h. The surface area was calculated using Brunauer−Emmett−Teller (BET) equation in the range P/P_0 < 0.3. The zeta potential was measured using a zeta potential analyzer (Brookhaven Instruments Corporation) in 10 mm polystyrene cuvettes at 25 °C. The hydrodynamic size distribution was estimated by dynamic light scattering (DLS) with a 90Plus/BI-MAS particle size analyzer (Brookhaven Instruments Corporation). Photoluminescence spectra were collected on a JASCO FP-6200 (400−700 nm) or Photon Technology International (200−900 nm) fluorescence spectrometer. The room-temperature magnetization curves were measured using a Quantum Designs MPMS-5S cryogenic susceptometer. The cell viability and hemolysis assays were measured using an iMark microplate reader (Bio-Rad).
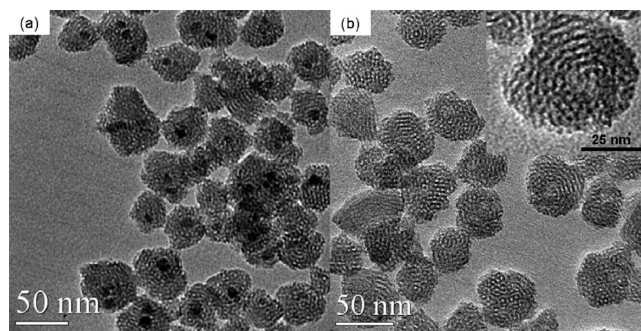
(26) Lin, Y.-S.; Tsai, C.-P.; Huang, H.-Y.; Kuo, C. T.; Hung, Y.; Huang, D.-M.; Chen, Y.-C.; Mou, C.-Y. *Chem. Mater.* **2005**, *17*, 4570.
(27) Lang, N.; Jorgensen, M.; Tuel, A. *Chem. Mater.* **2004**, *16*, 1961.

Scheme 1. Schematic Diagram of the One-Pot Synthetic Procedure to Produce PEG-Modified Fluorescent Mesoporous Silica NPs with Incorporated Fe₃O₄ NPs (Fe₃O₄@Dye-MSNs@PEG)
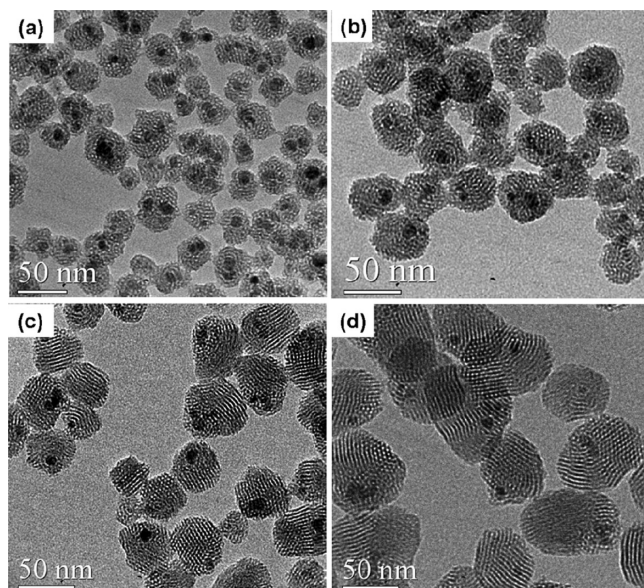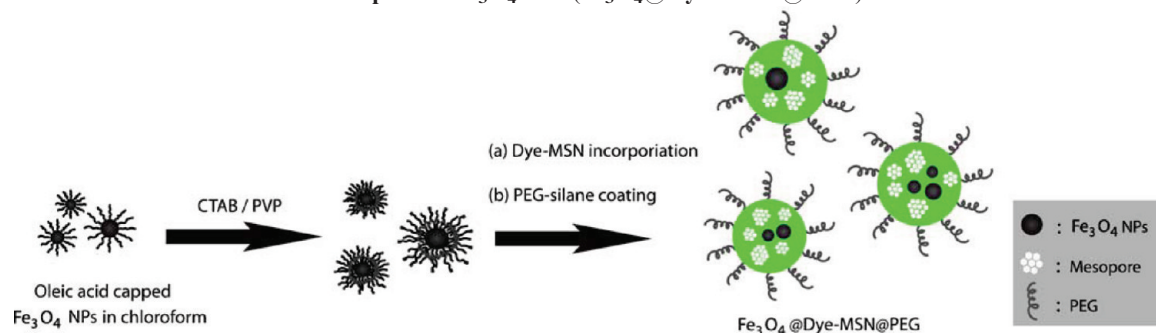
Figure 1. TEM images of surfactant-free Fe₃O₄@FITC-MSNs@PEG with varied diameters. (a) 33 ± 5.4 nm Fe₃O₄@FITC-MSNs@PEG, n = 180. (b) 42 ± 5.6 nm Fe₃O₄@FITC-MSNs@PEG, n = 125. (c) 53 ± 7.1 nm Fe₃O₄@FITC-MSNs@PEG, n = 100. (d) 67 ± 7.1 nm Fe₃O₄@FITC-MSNs@PEG, n = 130.

Figure 2. TEM images of surfactant-free (a) 42 nm Fe₃O₄@FITC-MSNs@PEG and (b) 42 nm H-FITC-MSNs@PEG.

Results and Discussion

The procedure for Fe₃O₄@Dye-MSNs@PEG synthesis is illustrated in Scheme 1. First, oleic acid-capped magnetite NPs were synthesized using a facile coprecipitation method. Compared to the thermal decomposition method developed by Sun et al.,[28] this simple synthesis not only utilizes inexpensive reactants but also generates a gram scale of products. The as-synthesized Fe₃O₄ NPs had an average nanoparticle diameter of 11 ± 3 nm (Figure S1 of the Supporting Information). The hydrophobic Fe₃O₄ NPs dispersed in chloroform were transferred to an aqueous phase by using *n*-cetyltrimethylammonium bromide (CTAB) and polyvinyl pyrrolidone (PVP) as stabilizing agents (Figure 1). The CTAB added in this step also serves as the porous structure-directing agent during the later silica condensation. PVP was incorporated into the synthesis of the Fe₃O₄ NPs as a cosurfactant for CTAB during the phase transfer to improve the transfer efficiency of the hydrophobic Fe₃O₄ NPs to the aqueous phase. In a pre-

vious report using CTAB as a stabilizing agent to transfer hydrophobic NPs to the aqueous phase, the transferred NPs needed to be filtered through a 0.44 μm syringe filter before silica coating, indicating that large aggregates were present in solution.[29] Without the addition of PVP, synthesized Fe₃O₄@Dye-MSNs@PEG included large aggregates of Fe₃O₄ NPs (Figure S2a). Upon filtering the PVP-free CTAB-Fe₃O₄ nanoparticle solution through a 0.44 μm syringe filter, a large amount of NPs were stuck in the filter (data not shown). In contrast, when PVP was added as a cosurfactant during synthesis, the aqueous phase CTAB- and PVP-stabilized Fe₃O₄ NPs passed through a 0.20 μm syringe filter with no observable aggregates. Additionally, no Fe₃O₄ aggregates were detected once incorporated into the silica NPs (Figure S2b). This result is not surprising since PVP is well-known as an amphiphilic polymer and, thus, can serve as a protecting agent for Fe₃O₄ NPs and improve their aqueous dispersity.[30]

The mesoporous silica nanostructure is formed around the aqueous Fe₃O₄ NPs by carefully controlling pH during the condensation reaction. During the mesoporous silica formation, the incorporation of dye molecules into the silica framework can be easily accomplished using a co-condensation method. Finally, to increase the water dispersity for biomedical applications, Fe₃O₄@Dye-MSNs were simultaneously modified with PEG-silane to prevent the binding of proteins and mini-

(28) Sun, S.; Zeng, H. *J. Am. Chem. Soc.* **2002**, *124*, 8204.

(29) Liong, M.; Lu, J.; Kovochich, M.; Xia, T.; Ruehm, S. G.; Nel, A. E.; Tamanoi, F.; Zink, J. I. *ACS Nano* **2008**, *2*, 889.

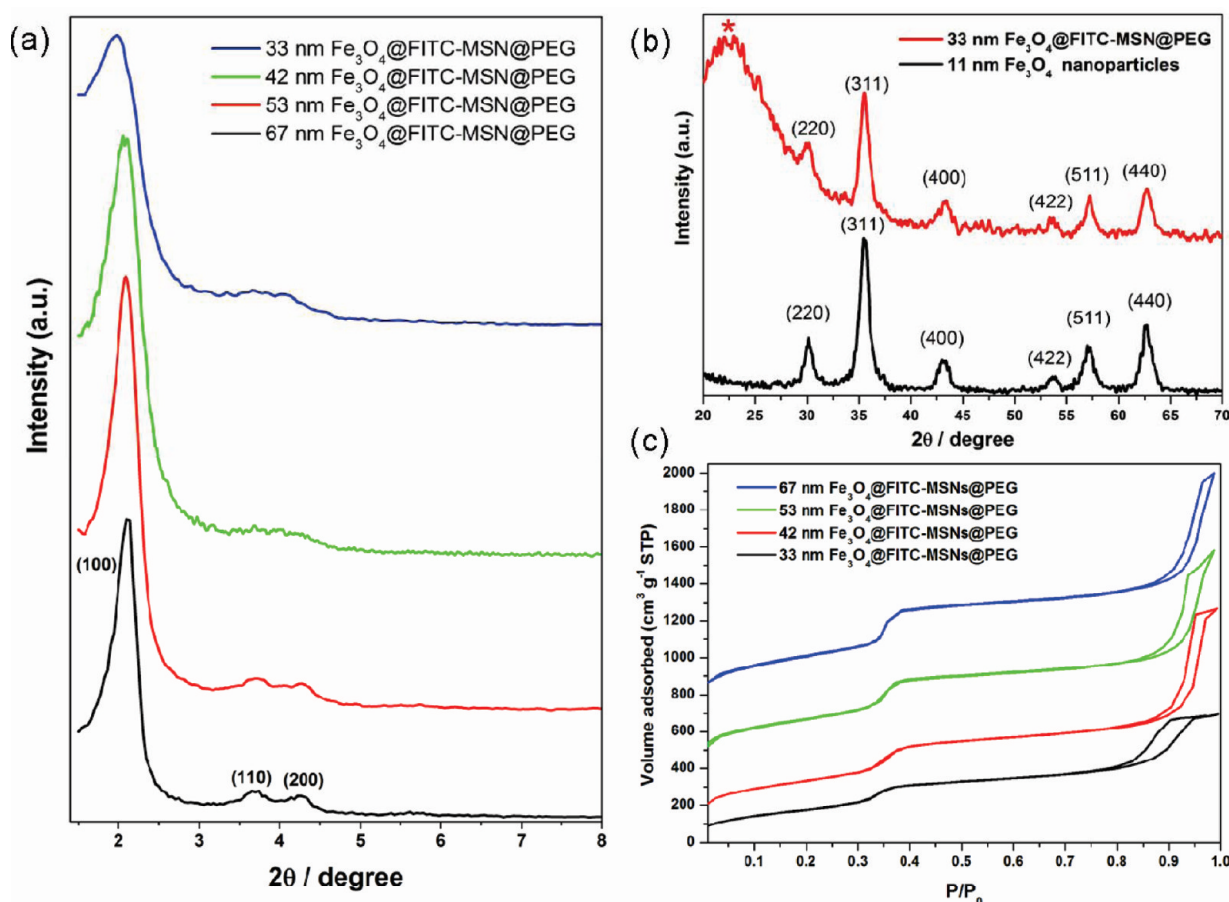(30) Graf, C.; Vossen, D. L.; Imhof, A.; Blaaderen, A. *Langmuir* **2003**, *19*, 6693.

Figure 3. Characterization of surfactant-free Fe_3O_4@FITC-MSNs@PEG. (a) Low-angle XRD patterns from Fe_3O_4@FITC-MSNs@PEG with varied diameters. (b) Wide-angle XRD patterns from as-synthesized 11 nm Fe_3O_4 and 33 nm Fe_3O_4@FITC-MSNs@PEG. The broad band (∗) at $2\theta = 23°$ originates from amorphous silica while (220), (311), (400), (422), (511), and (440) are characteristic magnetite peaks. (c) N_2 adsorption−desorption isotherms of Fe_3O_4@FITC-MSNs@PEG with varied diameters.

mize NP aggregation. Figure 1 demonstrates a variety of Fe_3O_4@FITC-MSNs@PEG sizes that can be synthesized using the methods detailed herein. As the ratio of the Fe_3O_4 NPs to silicate precursor used in the synthetic process is decreased, the resulting size of the Fe_3O_4-@FITC-MSNs@PEG increases, making it simple to control the overall nanoparticle size. To the best of our knowledge, this is the first report of the successful synthesis of multifunctional silica NPs with good aqueous dispersity having an average size smaller than 70 nm and still possessing a well-ordered mesoporous structure. Furthermore, because this work pursues an inexpensive and low temperature preparation of Fe_3O_4 NPs, dissolution of incorporated Fe_3O_4 NPs with acidic ethanol produces mesoporous silica NPs containing additional void space (Figure 2b) with a route that is easier and more economical than previously reported methods.[31,32] The high magnification TEM image of hollow FITC-MSNs is shown in Figure 2b. These hollow FITC-MSNs have an increased drug loading capacity due to the presence of both the hollow voids and the ordered mesopores.

The mesoporous ordering of Fe_3O_4@FITC-MSNs@PEG with varied diameters was examined using low-angle XRD from $2\theta = 1.5−8°$ (Figure 3a). The ordering of the porous structure increased as the concentration of Fe_3O_4 NPs decreased. The TEM images of 33 and 42 nm diameter Fe_3O_4@FITC-MSNs@PEG (Figure 1a and b) suggest short-range ordering and wormlike porous structures inside the NPs. The visual conclusions are supported by the broad and unresolved (110) and (200) XRD peaks detected when probing the 33 and 42 nm diameter Fe_3O_4@FITC-MSNs@PEG (Figure 3a). The sharp XRD patterns from 53 and 67 nm diameter Fe_3O_4-@FITC-MSNs@PEG indicate a very well-ordered 2D hexagonal mesoporous structure. This result confirms the long-range ordering of porous structure seen in TEM images (Figure 1c and d). The crystalline structure of Fe_3O_4 both before and after incorporation into Fe_3O_4-@Dye-MSNs@PEG was characterized using wide-angle XRD. As shown in Figure 3b, these patterns can be easily indexed to Fe_3O_4 by the International Centre for Diffraction Data powder diffraction file 98-000-0073 for magnetite. This result shows that the embedded Fe_3O_4 NPs retain their magnetite crystalline structure after template extraction. The N_2 adsorption−desorption isotherms for Fe_3O_4@FITC-MSNs@PEG with varied sizes exhibit the characteristic IV behavior for a well-developed

(31) Yang, J.; Lee, J.; Kang, J.; Lee, K.; Suh, J.-S.; Yoon, H.-G.; Huh, Y.-M.; Haam, S. *Langmuir* **2008**, *24*, 3417.
(32) Darbandi, M.; Thomann, R.; Nann, T. *Chem. Mater.* **2007**, *19*, 1700.

Table 1. Structural Properties and Saturation Magnetization Values of Surfactant-free Fe₃O₄@FITC-MSNs@PEG with Varied Sizes

samples	S_{BET} (m²/g)[a]	D_{BJH} (nm)[b]	V_t (cm³/g)[c]	saturation magnetization value at 300 K (emu/g)
33 nm Fe₃O₄@FITC-MSNs@PEG	694	2.4	1.08	12.0
42 nm Fe₃O₄@FITC-MSNs@PEG	885	2.4	1.95	6.27
53 nm Fe₃O₄@FITC-MSNs@PEG	948	2.4	1.49	3.18
67 nm Fe₃O₄@FITC-MSNs@PEG	1045	2.5	1.84	1.78

[a] S_{BET}: BET surface area calculated from data at $P/P_0 = 0.05-0.25$. [b] D_{BJH}: pore diameter assigned from the maximum on the BJH pore size distribution. [c] V_t: total pore volume calculated at P/P_0 at 0.99.
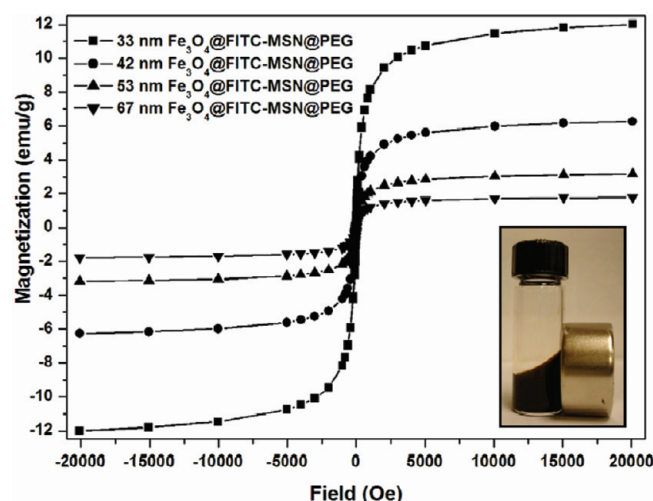
Figure 4. Magnetization curves at 300 K of surfactant-free Fe₃O₄-@FITC-MSNs@PEG with varied sizes. (inset) Photograph of the 35 mg/mL of 33 nm Fe₃O₄@FITC-MSNs@PEG solution during exposure to a magnet.

mesoporous structure, with a sharp capillary condensation at $P/P_0 \sim 0.35$ (Figure 3c). In addition, all samples have a secondary adsorption step (at $P/P_0 \sim 0.95$) that is attributed to the interparticle spaces formed between NPs after drying. All measured structural characteristics are listed in Table 1. All samples have high Brunauer–Emmett–Teller (BET) surface area (694–1045 m²/g) and large total pore volume (1.08–1.95 cm³/g). The decrease in surface area with decreased size is caused by the increasing volume fraction of magnetic NPs. Compared to recent reports,[19,20] the Fe₃O₄@FITC-MSNs@PEG synthesis detailed herein not only allows access to an average diameter smaller than 50 nm but also maintains the porous integrity and high surface area (885 m²/g). The vast improvement in achieved mesostructure, even in the small size regime, is likely due to the use of NH₄OH as a basic catalyst which favors formation of longer cylindrical silicate micelles within the Gouy–Chapman region.[33]

The Barret–Joyer–Halenda (BJH) method was applied to calculate the pore size distribution in all samples, indicating a maximum pore diameter of ∼2.4 nm. The magnetic behavior of Fe₃O₄@FITC-MSNs@PEG with varied diameters was measured using a magnetometer tuned from −20 000 to 20 000 Oe (Figure 4). No hysteresis was detected at 300 K for any of the samples, indicating

that the superparamagnetic behavior of the incorporated Fe₃O₄ NPs, an essential characteristic for T_2 MRI contrast agents, is intact. The high magnetic response is further demonstrated by applying a magnet to the outside of a vial containing the Fe₃O₄@FITC-MSNs@PEG aqueous solution (the inset of Figure 4). This high magnetization will facilitate the use of these multifunctional NPs as T_2 MRI contrast agents, in bioseparations, and in cell tracking. As shown in Table 1, the saturation magnetization value of Fe₃O₄@FITC-MSNs@PEG increases as the overall nanoparticle size decreases, further confirming the increasing Fe₃O₄ volume fraction. This volume fraction can be estimated by comparing the saturation magnetization values to that measured for the unincorporated 11-nm-diameter Fe₃O₄ NPs (60.0 emu/g, data not shown). The saturation magnetization value for the 33 nm diameter Fe₃O₄@FITC-MSNs-@PEG is 12.0 emu/g and, thus, the magnetic NP content is 20 wt %. Compared to recent reports,[12,14,19] the Fe₃O₄@FITC-MSNs@PEG NPs reported herein are not only smaller in size but also possesses much higher magnetization than previously reported nanomaterials.

The photoluminescence spectra of surfactant-free Fe₃O₄@FITC-MSNs@PEG and Fe₃O₄@RITC-MSNs@PEG exhibit the typical fluorescence emission of FITC and RITC (Figure 5a); this result confirms that the dye molecules can be anchored stably to the mesoporous silica framework after the surfactant extraction. Initial multifunctional NP syntheses focused on visible emission dyes, and in fact, different emission wavelengths were observed from Fe₃O₄@FITC-MSNs@PEG and Fe₃O₄@RITC-MSNs@PEG under UV illumination, as expected (Figure 5c). However, some applications of multifunctional biomedical NPs require fluorescent emission in the near-infrared (NIR) where the low light absorptivity of biological chromophores allows light to penetrate through several centimeters of tissue. Molecular dyes such as Cy5.5 and indocyanine green (ICG) are widely used in in vitro cell labeling and as NIR imaging contrast agents for in vivo deep-tissue imaging.[34] Hence, in addition to the previously mentioned visible region fluorophores, the NIR dye DyLight800 was incorporated into the multifunctional NPs. This was accomplished by reacting the primary amine groups from silica-bound aminopropyltrimethoxysilane with NHS-ester-activated DyLight800 fluorophores. The photoluminescence spectrum of surfactant-free Fe₃O₄@DyLight800-MSNs-

(33) Cai, Q.; Luo, Z. S.; Pang, W. Q.; Fan, Y. W.; Chen, X. H.; Cui, F. Z. *Chem. Mater.* **2001**, *13*, 258.

(34) Ke, S.; Wen, X.; Gurfinkel, M.; Charnsangavej, C.; Wallace, S.; Sevick-Muraca, E. M.; Li, C. *Cancer Res.* **2003**, *63*, 7870.
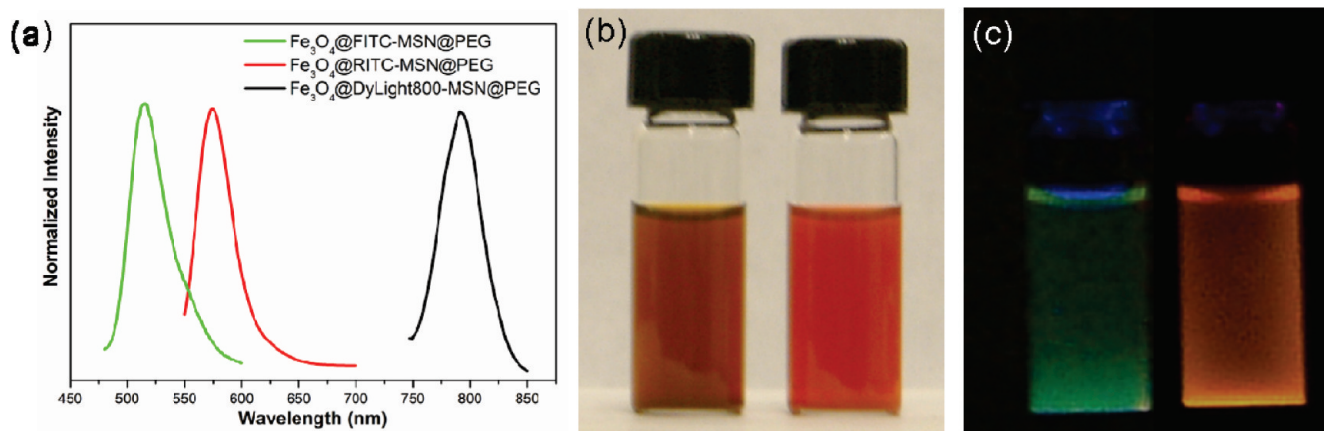
Figure 5. (a) Photoluminescence spectra of surfactant-free Fe_3O_4@FITC-MSNs@PEG (green line, λ_{ex} = 450 nm), Fe_3O_4@RITC-MSNs@PEG (red line, λ_{ex} = 525 nm), and Fe_3O_4@DyLight800-MSNs@PEG (black line, λ_{ex} = 720 nm). (b) Photographs of aqueous suspensions of Fe_3O_4@FITC-MSNs@PEG and Fe_3O_4@RITC-MSNs@PEG NPs. (c) Under UV illumination. The NPs presented excellent colloidal stability after template removal.
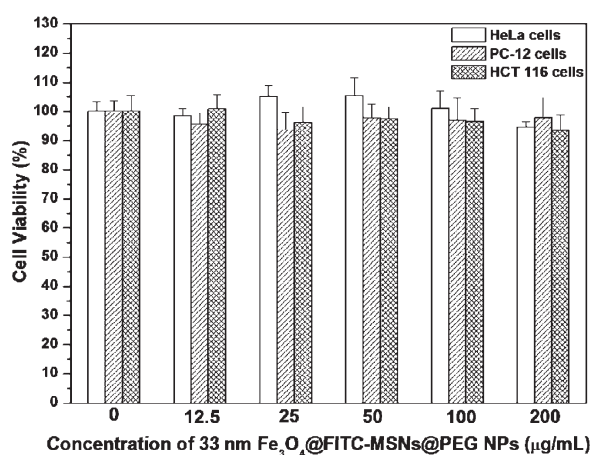

Figure 6. Cell viability of HeLa, PC-12, and HCT 116 cells using the MTT assay after treatment with different concentrations of 33 nm Fe_3O_4@FITC-MSNs@PEG NPs. Data represent to mean ± SD, n = 4.

@PEG showed the NIR dye was successfully incorporated into the silica wall by covalent bonding (Figure 5a). The PEG-silane was introduced into the synthetic procedure to enhance the colloidal stability. As is shown in Figure 5b, these surfactant-free NPs remained well-dispersed in deionized water without any visible aggregation after room temperature storage for 15 days. Dynamic light scattering (DLS) revealed that 33 nm diameter Fe_3O_4-@FITC-MSNs@PEG NPs have a hydrodynamic diameter of 57 ± 1 nm (Figure S3a in the Supporting Information) in deionized water and 73 ± 1 nm (Figure S3b) in PBS solution. The size difference between TEM and DLS measurements is attributed to the hydration sphere and outer PEG layer. Zeta potential measurement showed that 33 nm diameter Fe_3O_4@FITC-MSNs-@PEG NPs have a surface charge of −24 ± 2 mV in deionized water, further supporting the conclusion that a stable suspension is formed. The hydrodynamic diameter stability of 33 nm Fe_3O_4@FITC-MSNs@PEG in deionized water and PBS solution were measured at different times. There is no significant size change detected either in deionized water or PBS (Figure S3c), further supporting the absence of nanoparticle aggregation. The photo-

graphs of 33 nm Fe_3O_4@FITC-MSNs@PEG NPs in deionized water and PBS solution (Figure S3d) visually confirms the excellent dispersity and high colloidal stability, because no particle precipitation is observed.

Initial evaluation of the in vitro biocompatibility of 33 nm Fe_3O_4@FITC-MSNs@PEG NPs was performed using the MTT viability and hemolysis assays. MTT results showed that HeLa, PC-12, and HCT-116 cell viability were not affected even with 12 h exposures of up to 200 μg/mL NPs (Figure 6). In addition to the MTT assay, because the Fe_3O_4@Dye-MSNs@PEG NPs are designed for intravenous administration, it is important to test the compatibility of these multifunctional NPs with blood cells. In addition to the multifunctional nanoparticles that make up the focus of this manuscript, two other types of commonly used silica NPs, nonporous Stöber and Fe_3O_4@SiO_2 core−shell NPs, (Figure S6 of the Supporting Information) were synthesized to facilitate comparison of hemolytic activity with that of 33 nm Fe_3O_4@FITC-MSNs at different concentrations from 12.5 to 1000 μg/mL for 3 h. Typically, a large dose of NPs is used to achieve enough imaging contrast and therapeutic efficacy. Hence, the RBCs were incubated with NPs at a high concentration, up to 1000 μg/mL. As shown in Figure 7a, no hemolysis of RBCs was caused by 33 nm Fe_3O_4@FITC-MSNs at a concentration up to 100 μg/mL, but over 90% of RBCs were lysed by nonporous Stöber and Fe_3O_4@SiO_2 core−shell NPs (Figure 7b) at a concentration of 50 μg/mL. In the case of 33 nm Fe_3O_4@FITC-MSNs, detectable release of hemoglobin was observed at concentrations over 200 μg/mL (Figure S6). However, even after 3 h incubation, only 20% hemolysis was observed from 33 nm Fe_3O_4@FITC-MSNs. This is likely due to the lower number density of silanol groups on the surface of mesoporous silica shell compared to that of the solid silica nanoparticles. As a separate control, pure Fe_3O_4 NPs showed no hemolytic effect on RBCs (data not shown), indicating that the unlikely liberation of the magnetic center from the multifunctional nanoparticles would not be problematic.
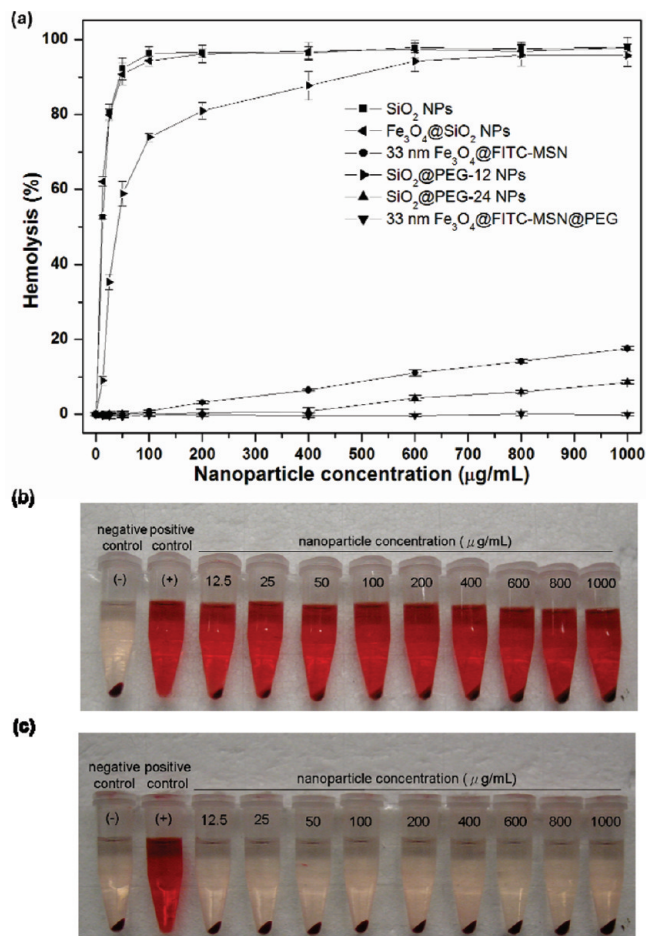
Figure 7. (a) Concentration-dependent hemolysis of Stöber SiO$_2$ NPs (square), Fe$_3$O$_4$@SiO$_2$ NPs (left pointing triangle), 33 nm Fe$_3$O$_4$@FITC-MSN (circle), Stöber SiO$_2$@PEG-12 NPs (right pointing triangle), Stöber SiO$_2$@PEG-24 NPs (upward pointing triangle), and 33 nm Fe$_3$O$_4$@-FITC-MSN@PEG (downward pointing triangle). Photographs of RBCs incubated with (b) Fe$_3$O$_4$@SiO$_2$ and (c) Fe$_3$O$_4$@FITC-MSNs@PEG at different concentrations for 3 h. The red hemoglobin release from damaged RBCs was determined by the supernatants. Data represent to mean ± SD, $n = 4$.

While these measurements clearly reveal that the mesoporous silica coating greatly reduces the hemolytic activity of silica NPs compared to the nonporous silica coating, further blood compatibility can be promoted via surface modification of either porous or nonporous silica NPs.[23] Herein, PEG-silane was used to eliminate the silanol groups on the surface of nonporous Stöber SiO$_2$ NPs and 33 nm Fe$_3$O$_4$@FITC-MSNs. Nonporous Stöber SiO$_2$ NPs were reacted with PEG-silane in two different periods, 12 and 24 h. The resulting PEG-coated silica NPs are referred to as SiO$_2$@PEG-12 and SiO$_2$@PEG-24, with expected variations in PEG coverage and ordering. Compared to the 12 h PEG-silane coating, the hemolytic activity of nonporous Stöber SiO$_2$ NPs was greatly reduced with 24 h PEG-silane coating; however, detectable hemolysis still can be seen at concentrations over 600 μg/mL. Contrary to SiO$_2$@PEG NPs, no hemolysis was observed after 3 h incubation with 33 nm Fe$_3$O$_4$-@FITC-MSNs@PEG at concentrations ranging from 12.5 to 1000 μg/mL (Figure 7a and c). This result further confirms that the surface silanol groups of Fe$_3$O$_4$@FITC-

MSNs are much fewer than nonporous Stöber SiO$_2$ NPs and can be eliminated by PEG modification. Finally, long-term hemolysis of RBCs was tested in the presence of 33 nm Fe$_3$O$_4$@FITC-MSNs@PEG at the concentration of 1000 μg/mL, and no significant hemolysis was detected even after 36 h incubation (Figure S8 of the Supporting Information), confirming the biocompatibility of 33 nm Fe$_3$O$_4$@FITC-MSNs@PEG.

Conclusions

In summary, this work demonstrates a one-pot size-controllable synthesis of multifunctional mesoporous silica NPs having well-ordered structure and large surface areas (700−1000 m^2/g), high magnetization (2−12 emu/g), PEG coating, and diameters less than 70 nm. Dissolution of embedded Fe$_3$O$_4$ NPs produces hollow mesoporous silica NPs as well. Visible fluorophores, NIR fluorophores, and magnetic NPs are all incorporated into the porous silica NPs without compromising the mesoporous structure to facilitate multimodal imaging. Importantly, these PEG-modified multifunctional mesoporous silica NPs exhibit excellent colloidal stability in both water and PBS solutions. MTT and hemolysis results further confirm their high biocompatibility. Compared to nonporous silica nanoparticles, mesoporous silica materials can not only reduce red blood cell membrane damage but also provide a large surface area for drug loading. We believe these biocompatiable multifunctional NPs have great potential for bioimaging and drug delivery applications.

Supporting Information Available: Synthesis details for Stöber SiO$_2$ NPs, Stöber SiO$_2$@PEG NPs and Fe$_3$O$_4$@SiO$_2$ NPs. Photographs of oleic acid capped Fe$_3$O$_4$ in chloroform and CTAB/PVP stabilized Fe$_3$O$_4$ NPs in water. TEM images of Fe$_3$O$_4$@FITC-MSNs@PEG without the addition of PVP and with the addition of PVP. Particle size distributions of surfactant-free Fe$_3$O$_4$@FITC-MSNs@PEG with varied diameters. DLS of surfactant-free 33 nm Fe$_3$O$_4$@FITC-MSNs@PEG NPs in deionized water and PBS solution. Hemolysis photograph of RBCs incubated with Fe$_3$O$_4$@FITC-MSNs at different concentrations. Time-dependent hemolysis of RBCs in the presence of 33 nm Fe$_3$O$_4$@FITC-MSNs@PEG. This material is available free of charge via the Internet at http://pubs.acs.org.